IEEE Photonics Journal
An IEEE Photonics Society Publication

Open Access

Efficient Optical Trapping and Detection of Nanoparticle Via Plasmonic Bowtie Notch

Volume 11, Number 2, April 2019

Yi-Chang Lin
Po-Tsung Lee, *Member, IEEE*

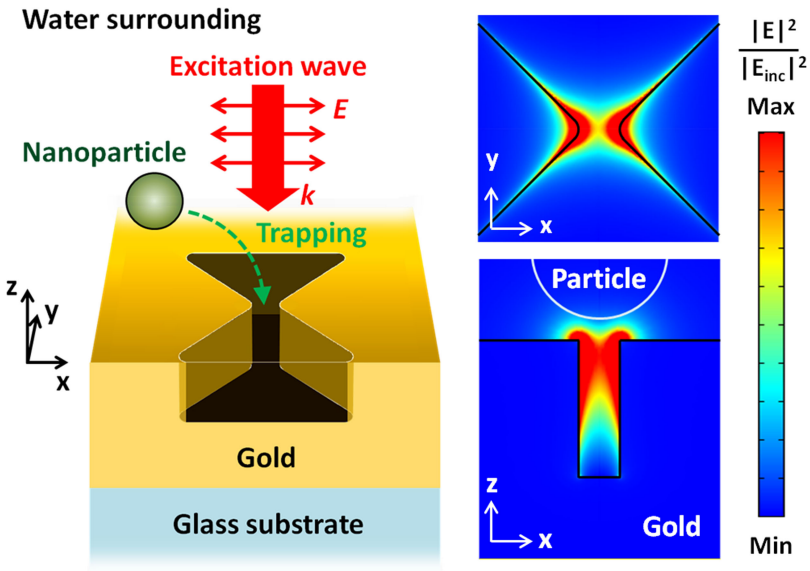

DOI: 10.1109/JPHOT.2019.2907273
1943-0655 © 2019 IEEE

IEEE photonics SOCIETY

IEEE

Efficient Optical Trapping and Detection of Nanoparticle Via Plasmonic Bowtie Notch

Yi-Chang Lin and Po-Tsung Lee, *Member, IEEE*

Department of Photonics, College of Electrical and Computer Engineering, National Chiao Tung University, Hsinchu 30010, Taiwan

DOI:10.1109/JPHOT.2019.2907273

Manuscript received February 22, 2019; revised March 12, 2019; accepted March 21, 2019. Date of current version April 3, 2019. This work was supported by the Research Team of Photonic Technologies and Intelligent Systems at the National Chiao Tung University within the framework of the Higher Education Sprout Project by the Ministry of Education and Ministry of Science and Technology (MOST) under Contract number MOST 106-2221-E-009-123-MY3, Taiwan. Corresponding author: Po-Tsung Lee (e-mail: potsung@mail.nctu.edu.tw).

Abstract: For manipulating nanoparticles, we propose a nanotweezer named plasmonic bowtie notch (PBN) by adding a thin metal film to the bottom of plasmonic bowtie aperture. The PBN can exert a large trapping force on nanoparticle because the enhanced field of resonance mode can be much accessed by nanoparticle. The optical properties and factors influencing trapping force of PBN are fully investigated and discussed. The optimized PBN shows an excellent trapping capability with ultralow threshold excitation intensity of 0.64 mW/μm^2 for stable trapping of a 100 nm polystyrene particle. In addition, it provides a label-free detection of the trapped particle by observing the extinction spectrum. The sensitivity to trapped target size of 71 pm redshift in peak wavelength per 1 nm increase of particle size is relatively high compared with those obtained from most near-field tweezers. Furthermore, the footprint of PBN is only 200 nm $\times$ 220 nm. The capabilities of the proposed design show a great potential in the application of nanoparticle trapping and sensing.

Index Terms: Optical tweezers, plasmonic nanostructure, bowtie aperture, optical sensing, nanoparticles.

1. Introduction

The optical tweezers, firstly introduced by Ashkin *et al.*, have opened a revolutionary method to manipulate tiny neutral particles [1]. By utilizing a single-highly-focused laser beam, the high optical intensity gradient around focal spot exerts trapping force on particle toward focus. This technique provides non-invasive and damage-free handling of particles with three-dimensional degree of freedom. Also, it has inspired many applications in areas of physical and biological sciences. Especially, optical tweezers have been widely applied in biology, such as manipulating live cells [2]–[4] and examining mechanical properties of many types of molecules [5]–[7]. Above discoveries provide us advanced understanding to the nature of fundamental bio-molecules. However, the system of free-space optical tweezers is always massive because of assembly of multiple optical components to achieve a good focused spot. Also, the diffraction-limited focused spot has difficulty in trapping of submicron particles with proper powers without damaging them [1]. An alternative configuration, known as near-field tweezers, can overcome the obstacles above. People found that the subwavelength sized evanescent fields surrounding dielectric or metallic structures can

offer a steep and enhanced intensity gradient [8], [9]. By employing structures with well designed evanescent fields, submicron particles can be rigidly trapped under practical input power. Also, these devices can be fabricated with chip size, which largely shrinks system volume. By further integrating with microfluidic channel, the devices give diversity for precise manipulating particles at chip scale.

As people seek for the tweezers with capability of efficient nanoparticles trapping, the equation of gradient force F_{grad} on spherical Rayleigh particle provides a design direction [1]:

$$F_{grad} = -\left(n_b^3 r^3/2\right)\left(m^2 - 1/m^2 - 2\right)\nabla E^2, \tag{1}$$

where n_b is the refractive index of surrounding medium, r is the radius of spherical particle, E is the electric field, and m is the ratio of the refractive index of particle (n_p) to n_b. As the force strength is proportional to the gradient of electric (E)-field intensity, optical energy should be condensed as tightly as possible to generate high field intensity and thus large trapping force. For dielectric structures, various designs such as photonic crystal (PhC) cavities [10]–[14] have been proposed and demonstrated for optical trapping of submicron or nanosized particles. However, certain number of PhC periods surrounding cavity is needed to produce greatly confined resonance modes, which results in the device length up to several micrometers. On the other hand, a much compact device can be attained by utilizing metallic structures due to the beyond-diffraction-limit confinement of plasmonic modes. There are works utilizing forces on particles induced by the surface plasmon polariton (SPP) modes on the surface of metal film [15], [16], stripe [17], and nanowire [18], [19]. But it is hard to make the particles stay at a fixed position because of the propagating nature of SPP mode (unless using two counterpropagating waves [17], [18]), and the mode energy is less concentrated in horizontal direction which may lead to limited trapping capability. For the localized surface plasmon resonance (LSPR) mode, the optical energy is localized and highly concentrated around the metallic nanostructures. As a result, high field intensity can be easily achieved. To obtain large trapping force, a variety of nanostructures has been proposed to condense optical energy into nanosized region and attain large field intensity, such as nanodots [20], nanoblock pair [21], dipole antennas [22], [23], bowtie antennas [24], [25], double nanohole [26], [27], and bowtie nanoapertures [28]–[30].

The dielectric and metallic tweezers discussed above successfully generate great field intensity and exert strong trapping force on particles, but large fraction of mode energy and highest field intensity actually located inside either dielectric core, transparent substrates, or tens of nanometer sized void region. If more energy could distribute at water surrounding and become accessible to trapping targets, we believe the trapping capability could be largely improved. To achieve this purpose, there are reports working on the re-distribution of the LSPR mode [31], [32]. In this paper, we propose a metallic nanotweezer named plasmonic bowtie notch (PBN) by adding a metal film to the bottom of plasmonic bowtie aperture (PBA) to realize efficient optical trapping of nanoparticle. Among all plasmonic nanostructures, PBA is frequently selected as trap unit because it possesses lightning-rod and gap effects that enhance the LSPR around the gap, which exerts large trapping force on target. With the help of addition of a metal film, we believe the field of LSPR of PBN would be more accessible to trapping target and thus a further enhanced trapping force can be obtained. Furthermore, the resonance characteristic of PBN can provide extinction spectral peak for particle detection. The event of nanoparticle trapping can be easily known by the peak shift of reflection extinction spectrum instead of complex imaging method. The factors for enhancing trapping force and the optical properties of PBN will be thoroughly investigated and discussed in this study.

2. Device Design and Simulation Setup

The proposed design is composed of an Au bowtie aperture on top of an Au film with thickness t, and the whole metal structure is supported on a glass substrate (n = 1.45), as illustrated in Fig. 1(a). The aperture is with length L in y direction, gap size g, depth H, and angle of bowtie θ fixed as 90°. The dielectric constant of Au is fitted using Lorentz-Drude model [33]. The device is assumed to be immersed in water surrounding (n = 1.33) as in real situation for suspending trapping targets.

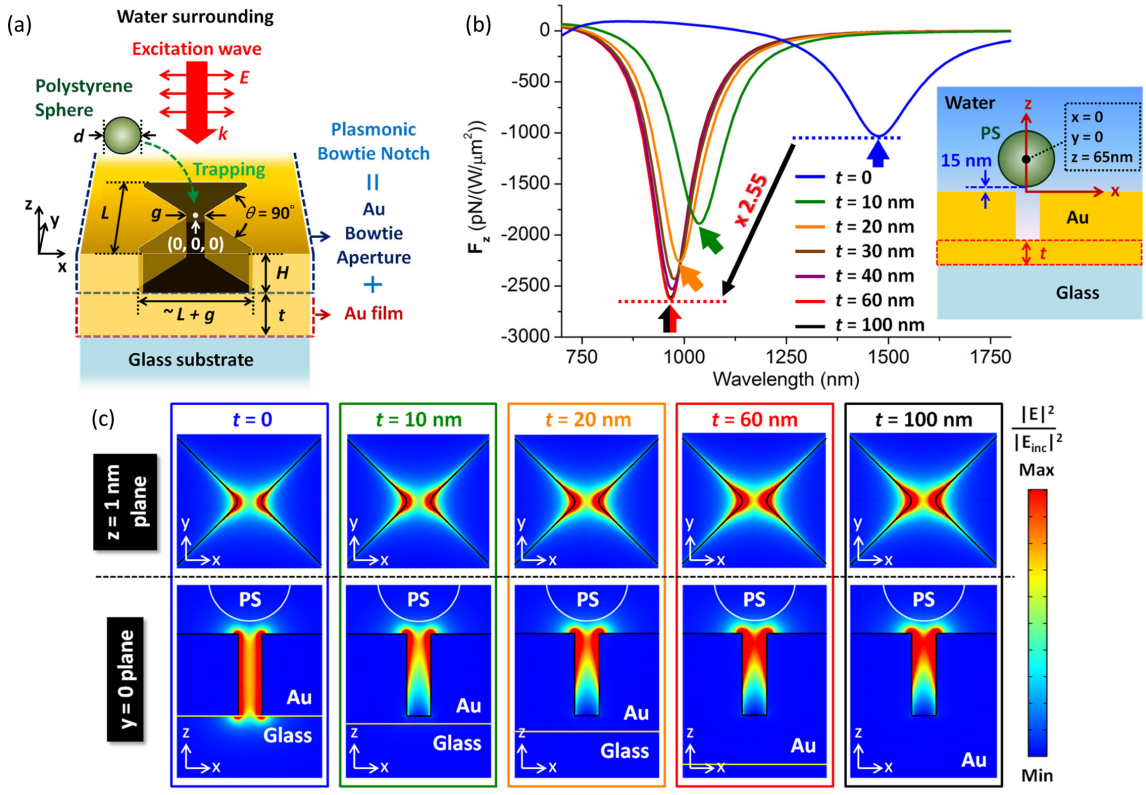

Fig. 1. (a) Schematic illustration of the proposed PBN composed of Au bowtie aperture and Au thin film on a glass substrate. (b) The spectra of F_z experienced by an 100 nm PS provided by PBA ($t = 0$) and PBNs with different t. Inset shows the position of 100 nm PS placed above the gap of structure. Blue, green, orange, red, and black arrows indicate the dip wavelengths of F_z spectra provided by structures with $t = 0$, 10, 20, 60, and 100 nm. (c) The E-field intensity enhancement distributions of PBA ($t = 0$) and PBNs with $t = 10$, 20, 60, and 100 nm. All distributions are obtained at the dip wavelengths of F_z spectra indicated by the arrows in (b).

Trapping target is chosen as polystyrene sphere (PS, n = 1.59) with diameter (d) of 100 nm, which is widely used in numerical evaluation for mimicking bio-targets such as viruses. The origin of x-y plane is set at the center of bowtie and the plane of z = 0 is on the top surface of Au layer. We perform three-dimensional finite element method in all simulations based on commercial software COMSOL Multiphysics to explore the optical properties of plasmonic structures. We apply the RF module to calculate the electromagnetic field distribution in steady state. All the external boundaries of the simulation domain are surrounded by perfectly matched layers (PMLs). A plane wave with E-field polarized in x direction is normally illuminated at the top surface of Au layer from water surrounding to excite the resonance mode [see Fig. 1(a)]. In all simulations, six apexes of bowtie are rounded with 10 nm in radius in the x-y plane considering fabrication feasibility. The corners in vertical direction remain un-rounded for simplification of modeling. It is worthy to note that when sharp corners are rounded, although field intensity becomes lower, mode distribution becomes more extended to the surrounding. As a result, the trapping force is enlarged [25]. Then the optical force on particle is obtained through postprocessing. As the particle encounters dramatic field distribution variation, the forces are evaluated using Maxwell stress tensor without approximation [34]. Since the simulation results are in steady state, we obtain the total force F on particle by integrating the time-averaged Maxwell stress tensor on the surface enclosing the particle:

$$F = \oint (\langle T_M \rangle \cdot \hat{n})\, dS, \tag{2}$$

where $\langle T_M \rangle = \langle D E^* + H B^* - \frac{1}{2}(D \cdot E^* + H \cdot B^*) I \rangle$ represents the time-averaged Maxwell stress tensor, $\hat{n}$ is the unit vector perpendicular to the integration surface, B is the magnetic flux density, D is the electric displacement, H is the magnetic field, and I is the isotropic tensor.

3. Characteristic Study

First, the trapping capabilities of PBN and PBA are evaluated. To ensure fair comparison, we set $L = 200$ nm, $g = 30$ nm, and $H = 100$ nm for both PBA and PBN. The only difference between PBN and PBA is that PBN is with an addition of Au bottom film. The single PS is placed above the gap of bowtie with a 15 nm separation from the top surface of Au layer (centered at coordinate (0, 0, 65 nm)) in both structures, shown as the inset of Fig. 1(b). The spectra of vertical trapping force (F_z, the optical force component in z direction) provided by structures with different film thicknesses t (ranging from 0 to 100 nm) are shown in Fig. 1(b). The force is normalized by the intensity of excitation wave in unit of W/μm^2. The dip in each spectrum represents the occurrence of LSPR excitation. At the dip wavelength, the enhanced field of LSPR mode distributed around the gap induces strong trapping force on PS toward the gap. Fig. 1(c) shows the E-field intensity enhancement distributions at dip wavelengths for structures with $t = 0$, 10, 20, 60, and 100 nm. When PBA ($t = 0$) evolves into PBN with $t = 10$ nm, an obvious maximum F_z strength enhancement and blueshift of spectrum are observed. If t is further increased, the maximum F_z strength and spectrum blueshift keep increasing until $t = 60$ nm owing to two effects provided by the addition of Au film. First, the film acts as a mirror and reflects the wave used to transmit through aperture. The reflected wave is re-coupled with the gap of structure and the resonance field is enhanced. Second, the screening effect offered by Au film pushes the induced charges vertically away from the bottom of notch. As induced charges tend to accumulate around the gap of bowtie structure due to gap and lightning-rod effects, they can be further compressed to the top surface of PBN. As a result, more fraction of mode energy is concentrated around the two top corners at gap region, which can be more accessible to trapping targets. But for PBA, charges evenly distribute along the sidewalls at gap region. Therefore, the mode energy also uniformly distributes along sidewalls and is hard to be accessed by target. Fig. 1(c) shows that PBNs are indeed with higher field intensities at the two top corners than the PBA. Accordingly, the LSPR mode of PBN can induce stronger trapping force on PS than the one of PBA. Since the two effects provided by the bottom Au film increase as t increases, the field intensity at top corners and hence the maximum strength of F_z increase with t, which can be observed in Fig. 1(b) and (c). On the other hand, more charges being pushed toward the top surface of PBN weakens plasmon coupling within the gap, so the dip wavelength of PBN is shorter than the one of PBA and blueshifts as t increases owing to the stronger screening effect. When t is larger than 60 nm, the spectrum of F_z remains nearly unchanged because the influences of the two effects saturate and reach their maxima. This can be supported from the almost the same intensity distributions of $t = 60$ and 100 nm in Fig. 1(c). Thus, the effect of substrate to PBN as t is thicker than 60 nm can be neglected and the substrate can be replaced by other materials. To conclude, PBN with the help of addition of Au film clearly exhibits much better trapping capability than PBA. The strength of F_z at dip wavelength by PBN is 2.55 times stronger than that by PBA. In the following discussions, t of PBN is chosen as 60 nm for fabrication consideration.

Next, we investigate the optical properties of PBN by tuning the parameters L and g. The schematic illustration of simulation settings is shown in Fig. 2(a). Single 100 nm PS is used to evaluate trapping force and placed at the same position above the gap (centered at coordinate (0, 0, 65 nm)). Here, H is fixed as 100 nm. We set different combinations of L (from 100 to 600 nm) and g (from 5 to 50 nm) to observe the variation of F_z spectrum. All spectra are obtained above the wavelength of 620 nm to avoid the interband transitions in Au [23]. Simulation shows that there is only single dip in each spectrum due to the excitation of LSPR, confirmed by examining the intensity distribution at dip wavelength. Fig. 2(b) and (c) show the dip wavelength (λ_{dip}) and the strength of F_z at dip wavelength ($|F_z|$ at λ_{dip}) in each spectrum. λ_{dip} increases as either L increasing or g decreasing, which can be explained by the variation of plasmon coupling within PBN.

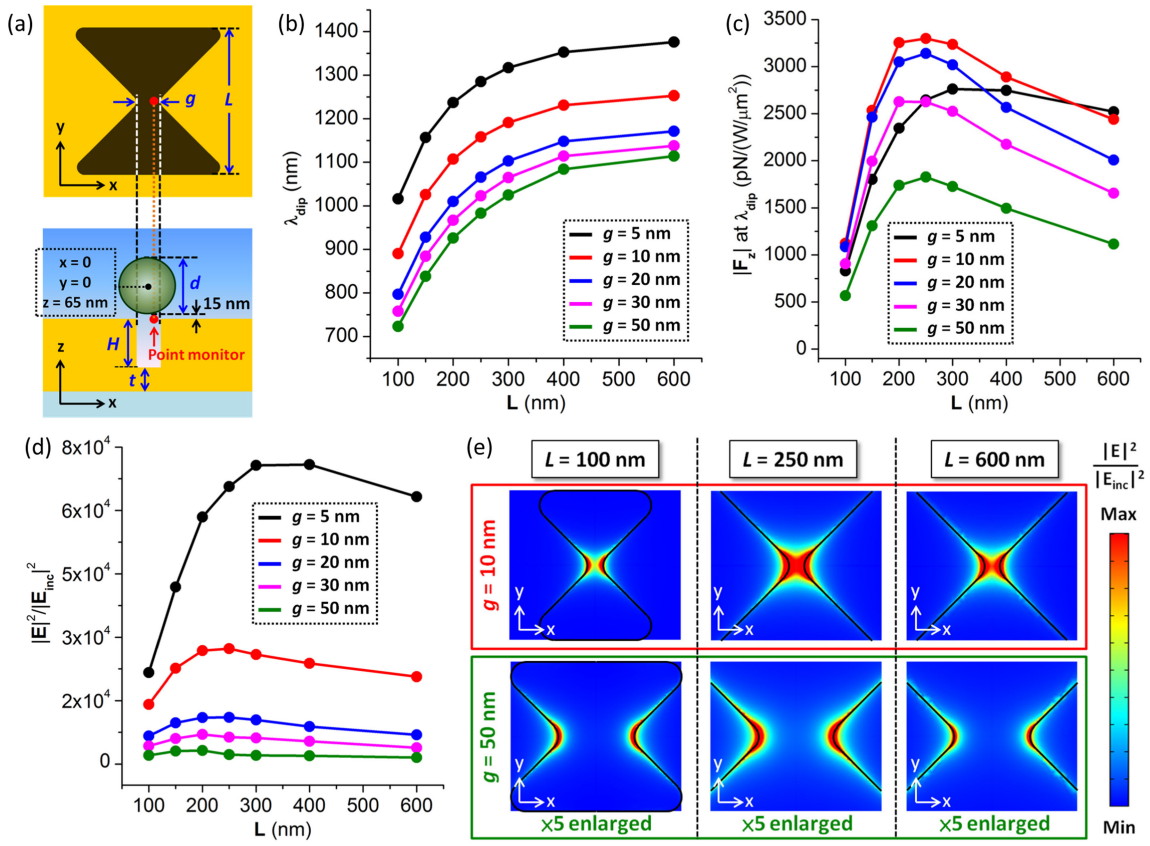

Fig. 2. (a) Schematic illustration of simulation settings for investigating the optical properties of PBN with different combinations of L and g. The position where intensity enhancement is monitored is at coordinate (g/2 - 1 nm, 0, 0), indicated by red dot. (b) Variation of dip wavelength in each F_z spectrum of PBN with different combinations of L and g. (c) Variation of F_z strength at dip wavelength of PBN with different combinations of L and g. (d) Variation of intensity enhancement at monitor point of PBN with different combinations of L and g. (e) Intensity enhancement distributions of PBN at the plane of z = 1 nm with combinations of L = 100 nm, 250 nm, 600 nm and g = 10 nm, 50 nm. The values for g = 50 nm are 5 times enlarged for better viewing.

Under fixed L, smaller g gives rise to stronger plasmon coupling between sidewalls at gap region because of the gap effect. And under fixed g, more charges can be induced by incident wave as L increases, also causing stronger plasmon coupling. From Fig. 2(c), there is always an optimal L for $|F_z|$ at λ_{dip} under fixed g, and $|F_z|$ at λ_{dip} increases as g decreases from 50 to 10 nm. But when g further decreases to 5 nm, most $|F_z|$ at λ_{dip} surprisingly decrease. Generally, higher field intensity should induce stronger trapping force. Thus, we monitor the intensity enhancement of each PBN at the position where the greatest field intensity occurs, as indicated in Fig. 2(a). Under fixed g, the variation of intensity enhancement reveals a similar trend as the one of $|F_z|$ at λ_{dip}, as shown in Fig. 2(d). To explain the variation of intensity enhancement, we can use the distribution of induced charges around the gap of PBN. Higher local charge density leads to higher local field intensity. The capability of accumulating charges around the gap depends on not only the gap and lightning-rod effects. The screening effect from the outer ring of notch also pushes charges to the central apexes of PBN. The pushing on charges is stronger when charges are closer to the outer ring of notch. Charges tend to more tightly accumulate around the gap for PBN with shorter L. But fewer charges are induced, which eventually leads to low local charge density. On the other hand, PBN with longer L can induce more charges. But the charges tend to loosely distribute along the lateral edges around the gap, which also results in low local charge density. As a result, there is

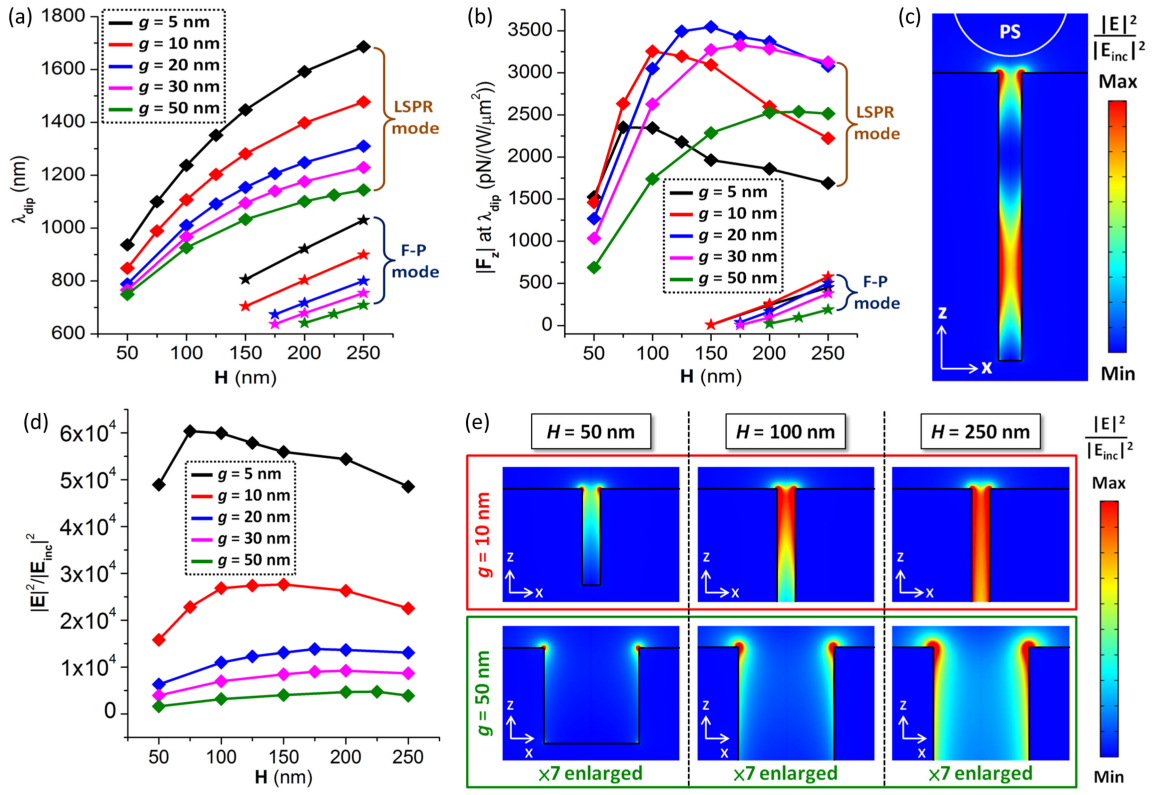

Fig. 3. (a) Variation of dip wavelength in each F_z spectrum for PBN with different combinations of H and g. The groups of LSPR and F-P modes are indicated. (b) Variation of F_z strength at dip wavelength for PBN with different combinations of H and g. The groups of LSPR and F-P modes are indicated. (c) Intensity enhancement distribution of the F-P mode at the plane of y = 0 for PBN with $H = 250$ nm and $g = 20$ nm. (d) Variation of intensity enhancement of the LSPR mode for PBN with different combinations of H and g. The value is obtained at the same monitor point indicated in Fig. 2(a). (e) Intensity enhancement distributions of the LSPR mode at the plane of y = 0 for PBN with combinations of $H = 50$ nm, 100 nm, 250 nm and $g = 10$ nm, 50 nm. The values for $g = 50$ nm are 7 times enlarged for better viewing.

an optimal L under fixed g for largest charge density accumulated at the two top corners around the gap of PBN and thus highest intensity enhancement, which can be observed from Fig. 2(e). Under fixed L, intensity enhancement keeps increasing while g decreases due to the gap effect, as shown in Fig. 2(d). When g decreases, the capability of accumulating charges around the gap and the field intensity are enhanced. This variation does not totally match with the one of $|F_z|$ at λ_{dip}. The force experienced by the target with fixed size is determined by both the degree of target-field overlap and field intensity around the target. Although plasmonic nanostructure with smaller gap offers better mode confinement with higher field intensity, the degree of target-field overlap is lower. We can observe that the increase of intensity enhancement is more and more significant but the increase of $|F_z|$ at λ_{dip} becomes less and less obvious when g decreases. This is because the decrease of degree of target-field overlap slows down the increase of $|F_z|$ at λ_{dip}. When the influence of the degree of target-field overlap dominants, $|F_z|$ at λ_{dip} becomes smaller, which can be seen from Fig. 2(c) as g decreasing from 10 to 5 nm. From above investigations, PBN can induce strong trapping force with L in the range from 200 to 300 nm. In the following discussions, L of PBN is chosen as 200 nm for compact device footprint.

Last, we investigate the optical properties of PBN by setting different combinations of H (from 50 to 250 nm) and g (from 5 to 50 nm). Fig. 3(a) and (b) show λ_{dip} and $|F_z|$ at λ_{dip} in each spectrum. We observe that a second dip appears in spectrum when H is larger than 150 nm. By

examining intensity enhancement distributions, the dip with longer wavelength is caused by the LSPR mode and the one with shorter wavelength is by the Fabry-Pérot (F-P) mode. Fig. 3(c) shows the distribution at shorter λ_{dip} of PBN with $H = 250$ nm and $g = 20$ nm. Compared with the LSPR mode, this mode is with one addition node inside the gap as a result of the interference between forward and backward SPP modes. As SPP mode propagates along the sidewalls at gap region, severe propagation loss occurs due to metal absorption. The field intensity around the two top corners at gap region is less enhanced, which results in much weaker trapping force than those provided by the LSPR modes, as shown in Fig. 3(b). Therefore, we focus on the LSPR mode since it is more suitable for nanoparticle trapping than the F-P mode. λ_{dip} of the LSPR mode increases as either H increasing or g decreasing. Similar with the effect of increasing L, the induced charges increase when H increases, resulting stronger plasmon coupling within PBN, and thus spectrum redshift. And the redshift of spectrum caused by decreasing g is due to the gap effect. There is always an optimal H for $|F_z|$ at λ_{dip} for the LSPR mode under fixed g and the optimal H decreases as g decreases. When g decreases from 50 to 20 nm, $|F_z|$ at λ_{dip} is enhanced. But when g further decreases to 5 nm, most $|F_z|$ at λ_{dip} decline considerably. As discussed above, the trapping force provided by PBN is influenced by the field distribution and intensity enhancement of the LSPR mode. As shown in Fig. 3(d), the trend of intensity enhancement variation under fixed g is similar with that of $|F_z|$ at λ_{dip}. And the intensity enhancement keeps increasing as g decreases, which is different from the trend of $|F_z|$ at λ_{dip} when g decreases from 20 to 5 nm. The variation of intensity enhancement is owing to the distribution of induced charges around the gap of PBN. The pushing on charges from the bottom of notch is stronger when charges are closer to the bottom. Therefore, charges tend to more tightly accumulate around the two top corners at gap region when PBN is with smaller H. However, fewer charges are induced, which leads to low local charge density. On the other hand, PBN with larger H can induce more charges. But the charges loosely distribute along the sidewalls at gap region, which also results in low local charge density. As a result, there is an optimal H under fixed g for largest charge density accumulated around the two top corners at gap region and thus highest intensity enhancement, which can be observed from Fig. 3(e). For $g = 10$ nm, the field intensity around the two top corners at gap region is strongly enhanced as H increases from 50 to 100 nm. When H further increases to 250 nm, the field intensity around top corners slightly decreases and more portion of mode energy distributes deeply inside the notch. For $g = 50$ nm, the field intensity around top corners keeps increasing as H increases from 50 to 250 nm. The evolution of intensity enhancement distribution is consistent with the behavior of induced charges. When g decreases, the intensity enhancement and the capability of accumulating charges are improved due to the gap effect. Induced charges can distribute more easily along the sidewalls at gap region, causing the decrease of optimal H. We can also observe that the mode field is more confined at gap region as g decreases, which leads to the decrease of the degree of target-field overlap. When g decreases from 50 to 20 nm, the increase of $|F_z|$ at λ_{dip} becomes smaller. And as g further decreases from 20 to 5 nm, the decrease of the degree of target-field overlap dominants over the increase of intensity enhancement, which causes the decrease of $|F_z|$ at λ_{dip}. The strongest $|F_z|$ occurs when $H = 150$ nm and $g = 20$ nm, and the corresponding λ_{dip} of 1154 nm falls in the range of 750 to 1200 nm, suitable for trapping bio-targets for minimized photo-damage to target [13]. The optimized PBN ($t = 60$ nm, $L = 200$ nm, $H = 150$ nm, and $g = 20$ nm) is with a very compact footprint of merely 200 $\times$ 220 nm.

4. Analysis of Particle Trapping and Sensing

The capability of nanoparticle trapping provided by the optimized PBN under fixed excitation wavelength of 1154 nm is analyzed. To know how stable the particle can be trapped, we assume that 100 nm PS is attracted toward the gap of PBN and stays above the gap with a 15 nm separation from the top surface of PBN. The black curve in Fig. 4(a) shows the evolution of optical force in x component (F_x) when the PS moves along the path in x direction with y = 0 and z = 65 nm. Since the field of LSPR mode highly concentrates around the gap of PBN, the direction of F_x always points to the center of bowtie and the equilibrium of F_x occurs at the position x = 0. We then integrate F_x

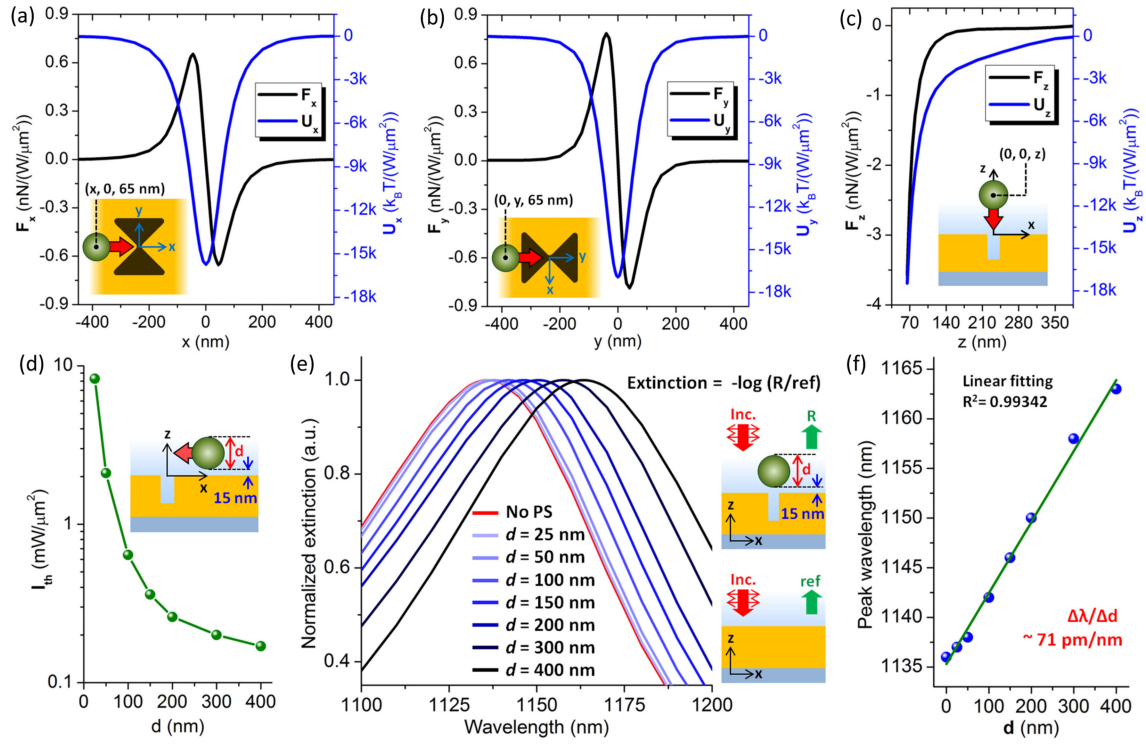

Fig. 4. (a) Evolution of F_x and distribution of U_x when PS moves along the path in x direction with y = 0 and z = 65 nm. (b) Evolution of F_y and distribution of U_y when PS moves along the path in y direction with x = 0 and z = 65 nm. (c) Evolution of F_z and distribution of U_z when PS moves along the path in z direction with x = 0 and y = 0. (d) Variation of I_{th} for stable trapping of PS with different sizes. (e) Variation of normalized extinction spectrum when PS with different sizes is trapped. (f) Variation of peak wavelength for different trapped PS sizes. The green line is the linear fitting to peak wavelength variation and its slope ($\Delta\lambda/\Delta d$) is 71 pm/nm. PS is assumed to be trapped above the gap with a 15 nm separation from the top surface of PBN in all cases.

along the path to obtain the optical potential experienced by the PS and the zero potential is set at infinite away from PBN. The blue curve in Fig. 4(a) shows the corresponding potential distribution in x direction (U_x). A criterion widely used for stable trapping requires the potential depth (ΔU) larger than $10\,k_BT$ for suppressing Brownian motion, where k_B is the Boltzmann constant and T is the system temperature [1]. Here we set T as room temperature 300 K. To compare with the energy of Brownian motion, U_x is arranged and normalized by the intensity of excitation wave in the unit of $k_BT/(\mathrm{W}/\mu\mathrm{m}^2)$. There is only single stable position with ΔU_x of $15739\,k_BT/(\mathrm{W}/\mu\mathrm{m}^2)$ at x = 0. Fig. 4(b) shows the trapping characteristics when the PS moves along the path in y direction with x = 0 and z = 65 nm. The direction of optical force in y component (F_y) also always points to the center of bowtie and the equilibrium of F_y occurs at the position y = 0. For the potential distribution in y direction (U_y), the deepest ΔU_y of $16929\,k_BT/(\mathrm{W}/\mu\mathrm{m}^2)$ happens at y = 0. Compared with Fig. 4(a), Fig. 4(b) shows larger maximum force strength and thus larger potential depth. This is because the resonance field is more extended in y direction leading to larger degree of target-field overlap. As a result, minimum excitation intensity of 0.64 $\mathrm{mW}/\mu\mathrm{m}^2$ is needed to achieve stable trapping of 100 nm PS at x = y = 0, where ΔU_x is $10\,k_BT$ and ΔU_y is $10.8\,k_BT$. The trapping characteristics in z direction are examined by moving the PS along the path in z direction with x = y = 0, as shown in Fig. 4(c). The direction of F_z is always toward the top surface of PBN and F_z becomes significantly stronger as the PS gets closer and overlaps more with the intense field. From the potential distribution in z direction (U_z), a ΔU_z of $11.1\,k_BT$ can be reached at z = 65 nm under excitation intensity of 0.64 $\mathrm{mW}/\mu\mathrm{m}^2$. Therefore, we confirm that single 100 nm PS can be stably

trapped at position x = y = 0, and z = 65 nm with threshold excitation intensity (I_{th}) of 0.64 mW/μm^2. The I_{th} for PS with different d are calculated and shown in Fig. 4(d). Because the force experienced by larger particle is stronger, the I_{th} decreases as d increases. The excitation intensity of PBN is relatively small compared to many prior works using particles with similar indices and sizes [1], [30]–[32]. At these ultralow excitation intensities, the thermal problem should be insignificant and would not disturb the trapping phenomenon. If necessary, the glass substrate can be replaced by a heat sink to ease the thermal problem [31], [32].

In addition to ultralow excitation intensity, PBN provides very precise nanoparticle trapping since there is only single hot spot at gap region. But it is hard to visually observe the trapping of targets with sizes below the diffraction limit. To solve this issue, targets labeled with fluorescent molecules are commonly used, which may influence the natural characteristic of the target and the fluorescent intensity would decay with time [13]. A label-free method for detecting the event of nanoparticle trapping is through the reflection extinction spectrum. Fig. 4(e) shows the normalized extinction spectra when trapping PS with different sizes ranging from 25 to 400 nm, and the spectrum without PS is also provided. All particles are assumed to be trapped above the gap with a 15 nm separation from the top surface of PBN. Because the LSPR mode experiences an increased effective index of surrounding when PS is trapped, there is a redshift of spectrum when trapping event occurs. The redshift of peak wavelength increases as PS size enlarges due to the increase of the effective index of surrounding. From the linear fitting result shown in Fig. 4(f), 71 pm redshift in peak wavelength per 1 nm increase of trapped PS size is achieved. This value is relatively larger than those obtained from many near-field tweezers [10], [11], [14]. Hence, we can detect the trapping event and recognize the size of trapped target by the amount of peak shift.

5. Conclusion

We propose a metallic nanotweezer named plasmonic bowtie notch, formed by adding an Au bottom film to the gold bowtie aperture, to achieve efficient optical trapping and detection of nanoparticle. The addition of the Au film makes the transmitted optical energy re-coupled with the gap and pushes induced charges to the two top corners at gap region. As a result, the field of LSPR mode of PBN is largely enhanced and concentrated around the two top corners, which is also more accessible to trapping target. The trapping force provided by PBN is 2.55 times stronger than that by PBA. The trapping force is influenced by not only field intensity around the two top corners but also the degree of target-field overlap. The variation of field intensity is related to the induced charges density at the two top corners, which is a result of lightning-rod effect, gap effect, and screening effect from the bottom and outer ring of notch. The influence of the degree of target-field overlap is more obvious when the gap size is varied due to the varied field confinement. Although a much small gap produces extremely high field intensity, the much confined mode causes lowered degree of target-field overlap, leading to declined trapping force. Single 100 nm PS can be stably and precisely trapped by optimized PBN under an ultralow threshold excitation intensity of 0.64 mW/μm^2. Moreover, PBN provides a label-free detection to the event of nanoparticle trapping by the redshift in the peak wavelength of extinction spectrum. A high sensitivity to trapped target size of 71 pm redshift in peak wavelength per 1 nm increase of trapped PS size is obtained. Furthermore, PBN is very compact with footprint of 200 nm $\times$ 220 nm. Our optimized design can provide efficient trapping and sensitive detection of nanoparticle, which can be a very useful tool in the researches of nanoscience, such as measuring the properties of nanoparticles [26], analyzing the interactions between bio-particles [12], and assembling nanomaterials [13], [30], [31].

References

[1] A. Ashkin, J. M. Dziedzic, J. E. Bjorkholm, and S. Chu, "Observation of a single-beam gradient force optical trap for dielectric particles," *Opt. Lett.*, vol. 11, no. 5, pp. 288–290, May 1986.
[2] A. Ashkin and J. M. Dziedzic, "Optical trapping and manipulation of viruses and bacteria," *Science*, vol. 235, no. 4795, pp. 1517–1520, Mar. 1987.

[3] A. Ashkin, J. M. Dziedzic, and T. Yamane, "Optical trapping and manipulation of single cells using infrared laser beams," *Nature*, vol. 330, pp. 769–771, Dec. 1987.
[4] A. Ashkin and J. M. Dziedzic, "Internal cell manipulation using infrared laser traps," *Proc. Nat. Acad. Sci. USA*, vol. 86, pp. 7914–7918, Oct. 1989.
[5] M. Kurachi, M. Hoshi, and H. Tashiro, "Buckling of a single microtubule by optical trapping forces: Direct measurement of microtubule rigidity," *Cell Motil. Cytoskeleton*, vol. 30, no. 3, pp. 221–228, 1995.
[6] Y. Tsuda, H. Yasutake, A. Ishijima, and T. Yanagida, "Torsional rigidity of single actin filaments and actin–actin bond breaking force under torsion measured directly by *in vitro* micromanipulation," *Proc. Nat. Acad. Sci. USA*, vol. 93, pp. 12937–12942, Nov. 1996.
[7] S. B. Smith, Y. Cui, and C. Bustamante, "Overstretching B-DNA: The elastic response of individual double-stranded and single-stranded DNA molecules," *Science*, vol. 271, no. 5250, pp. 795–799, Feb. 1996.
[8] D. Erickson, X. Serey, Y.-F. Chen, and S. Mandal, "Nanomanipulation using near field photonics," *Lab Chip*, vol. 11, no. 6, pp. 995–1009, Jan. 2011.
[9] M. L. Juan, M. Righini, and R. Quidant, "Plasmon nano-optical tweezers," *Nat. Photon.*, vol. 5, pp. 349–356, Jun. 2011.
[10] S. Lin, J. Hu, L. Kimerling, and K. Crozier, "Design of nanoslotted photonic crystal waveguide cavities for single nanoparticle trapping and detection," *Opt. Lett.*, vol. 34, no. 21, pp. 3451–3453, Nov. 2009.
[11] N. Descharmes, U. P. Dharanipathy, Z. Diao, M. Tonin, and R. Houdré, "Single particle detection, manipulation and analysis with resonant optical trapping in photonic crystals," *Lab Chip*, vol. 13, no. 16, pp. 3268–3274, Aug. 2013.
[12] P. Kang, P. Schein, X. Serey, D. O'Dell, and D. Erickson, "Nanophotonic detection of freely interacting molecules on a single influenza virus," *Sci. Rep.*, vol. 5, Jul. 2015, Art. no. 12087.
[13] Y.-F. Chen, X. Serey, R. Sarkar, P. Chen, and D. Erickson, "Controlled photonic manipulation of proteins and other nanomaterials," *Nano Lett.*, vol. 12, no. 3, pp. 1633–1637, Jan. 2012.
[14] S. Lin and K. B. Crozier, "Trapping-assisted sensing of particles and proteins using on-chip optical microcavities," *ACS Nano*, vol. 7, no. 2, pp. 1725–1730, Feb. 2013.
[15] G. Volpe, R. Quidant, G. Badenes, and D. Petrov, "Surface plasmon radiation forces," *Phys. Rev. Lett.*, vol. 96, no. 23, Jun. 2006, Art. no. 238101.
[16] K. Wang, E. Schonbrun, and K. B. Crozier, "Propulsion of gold nanoparticles with surface plasmon polaritons: Evidence of enhanced optical force from near-field coupling between gold particle and gold film," *Nano Lett.*, vol. 9, no. 7, pp. 2623–2629, Jul. 2009.
[17] K. Wang, E. Schonbrun, P. Steinvurzel, and K. B. Crozier, "Scannable plasmonic trapping using a gold stripe," *Nano Lett.*, vol. 10, no. 9, pp. 3506–3511, Sep. 2010.
[18] C. Cheng, X. Xu, H. Lei, and B. Li, "Plasmon-assisted trapping of nanoparticles using a silver-nanowire-embedded PMMA nanofiber," *Sci. Rep.*, vol. 6, Feb. 2016, Art. no. 20433.
[19] C. Yang, D. Pan, L. Tong, and H. Xu, "Guided transport of nanoparticles by plasmonic nanowires," *Nanoscale*, vol. 8, no. 46, pp. 19195–19199, Oct. 2016.
[20] A. N. Grigorenko, N. W. Roberts, M. R. Dickinson, and Y. Zhang, "Nanometric optical tweezers based on nanostructured substrates," *Nat. Photon.*, vol. 2, pp. 365–370, Jun. 2008.
[21] Y. Tanaka, S. Kaneda, and K. Sasaki, "Nanostructured potential of optical trapping using a plasmonic nanoblock pair," *Nano Lett.*, vol. 13, no. 5, pp. 2146–2150, Apr. 2013.
[22] M. Righini, P. Ghenuche, S. Cherukulappurath, V. Myroshnychenko, F. J. Garcıá de Abajo, and R. Quidant, "Nano-optical trapping of rayleigh particles and *escherichia coli* bacteria with resonant optical antennas," *Nano Lett.*, vol. 9, no. 10, pp. 3387–3391, Oct. 2009.
[23] W. Zhang, L. Huang, C. Santschi, and O. J. F. Martin, "Trapping and sensing 10 nm metal nanoparticles using plasmonic dipole antennas," *Nano Lett.*, vol. 10, no. 3, pp. 1006–1011, Mar. 2010.
[24] B. J. Roxworthy and K. C. Toussaint Jr, "Femtosecond-pulsed plasmonic nanotweezers," *Sci. Rep.*, vol. 2, Sep. 2012, Art. no. 660.
[25] P.-T. Lin, H.-Y. Chu, T.-W. Lu, and P.-T. Lee, "Trapping particles using waveguide-coupled gold bowtie plasmonic tweezers," *Lab Chip*, vol. 14, no. 24, pp. 4647–4652, Sep. 2014.
[26] Y. Pang and R. Gordon, "Optical trapping of a single protein," *Nano Lett.*, vol. 12, no. 1, pp. 402–406, Jan. 2012.
[27] Z. Xu, W. Song, and K. B. Crozier, "Direct particle tracking observation and Brownian dynamics simulations of a single nanoparticle optically trapped by a plasmonic nanoaperture," *ACS Photon.*, vol. 5, no. 7, pp. 2850–2859, Jul. 2018.
[28] N. M. Hameed, A. E. Eter, T. Grosjean, and F. I. Baida, "Stand-alone three-dimensional optical tweezers based on fibred bowtie nanoaperture," *IEEE Photon. J.*, vol. 6, no. 4, Aug. 2014, Art. no. 4500510.
[29] J. Berthelot, S. S. Aćimović, M. L. Juan, M. P. Kreuzer, J. Renger, and R. Quidant, "Three-dimensional manipulation with scanning near-field optical nanotweezers," *Nat. Nanotechnol.*, vol. 9, pp. 295–299, Apr. 2014.
[30] R. A. Jensen *et al.*, "Optical trapping and two-photon excitation of colloidal quantum dots using bowtie apertures," *ACS Photon.*, vol. 3, no. 3, pp. 423–427, Mar. 2016.
[31] Y. Zheng, J. Ryan, P. Hansen, Y.-T. Cheng, T.-J. Lu, and L. Hesselink, "Nano-optical conveyor belt, Part II: Demonstration of handoff between near-field optical traps," *Nano Lett.*, vol. 14, no. 6, pp. 2971–2976, Jun. 2014.
[32] K. Wang, E. Schonbrun, P. Steinvurzel, and K. B. Crozier, "Trapping and rotating nanoparticles using a plasmonic nano-tweezer with an integrated heat sink," *Nat. Commun.*, vol. 2, Sep. 2011, Art. no. 469.
[33] A. D. Rakić, A. B. Djurišić, J. M. Elazar, and M. L. Majewski, "Optical properties of metallic films for vertical-cavity optoelectronic devices," *Appl. Opt.*, vol. 37, no. 22, pp. 5271–5283, Aug. 1998.
[34] A. H. J. Yang and D. Erickson, "Stability analysis of optofluidic transport on solid-core waveguiding structures," *Nanotechnology*, vol. 19, no. 4, Jan. 2008, Art. no. 045704.